

Boosting Polysulfide Conversion in Lithium–Sulfur Batteries via Palladium-Based Environmentally Friendly Porous Catalyst

Tianhong Zhou,[§] Yan Zhao,[§] Kyung Seob Song,[§] Dominika Baster, Mario El Kazzi, and Ali Coskun*



Read Online

ACCESS |



Metrics & More

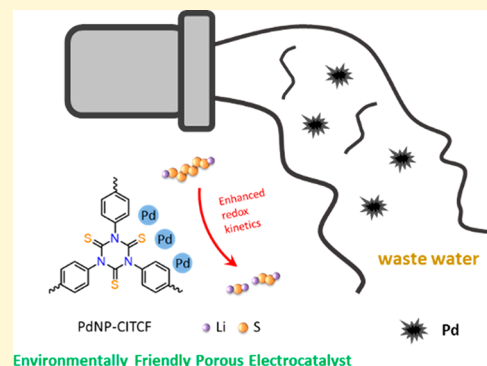


Article Recommendations



Supporting Information

ABSTRACT: Lithium–sulfur (Li–S) batteries offer a great potential as next-generation energy storage systems. However, the shuttling effect and the sluggish reaction kinetics of lithium polysulfides (LiPS) result in a low specific capacity and poor rate performance. In an effort to address these challenges, here, we demonstrate the use of captured Pd from wastewater conditions using porous polyisocyanurates, named covalent isothiocyanurate frameworks (CITCFs), bearing homogeneously distributed sulfur binding sites as a sustainable and environmentally friendly electrocatalyst to suppress the shuttling effect while promoting the kinetics of sulfur redox reactions. The designed electrocatalyst endows Li–S batteries with a high initial specific capacity of 907 mAh g⁻¹ at 1 C, stable capacity of 450 mAh g⁻¹ after 500 cycles at 1 C, and excellent rate performance with a capacity of 681 mAh g⁻¹ at 2 C, thus offering a new perspective for the sustainable development of electrocatalysts toward the realization of practical Li–S batteries.



1. INTRODUCTION

The rapid development of portable electronics and electric and hybrid-electric vehicles has led to a substantial interest in the development of high-energy-density rechargeable batteries.^{1–4} Among the various energy storage systems, Li–S batteries are considered to be one of the most promising candidates owing to their cost effectiveness, lightweight, high theoretical specific capacity (1672 mA h g⁻¹), and energy density (2600 Wh kg⁻¹).^{5,6} Despite these promising features, however, the practical implementation of the Li–S battery has been challenged by several limitations including Li-polysulfide (LiPS) shuttling, the insulating nature of S and its discharge products, volume expansion upon cycling, and sluggish kinetics of LiPS redox reactions.^{7,8} Multiple strategies have been employed to address these challenges for Li–S batteries.^{9,10} In this direction, many carbonaceous materials including graphene interlayers,¹¹ metal organic frameworks (MOFs),^{12–14} carbon hosts with high porosity,^{15,16} and functional carbon nanostructures^{17,18} have been introduced owing to their ability to physically trap LiPS and compensate for the electrical conductivity, large pore volume, or interlayer spaces. Whereas the physical adsorption of LiPS has been shown to increase the attainable capacity and cyclability to some extent, polarized LiPS species still tend to diffuse out of thick cathodes under high rate and long cycling conditions owing to the low affinity of these materials toward LiPS. Hence, metal oxides such as Al₂O₃, MnO₂, TiO₂, and Nb₂O₅ have emerged as promising alternatives owing to their strong affinity toward polysulfides.^{19–22} However, these oxides still suffer from low electrical conductivity and cannot

effectively convert accumulated LiPSs into Li₂S₂/Li₂S, thus, resulting in sluggish redox kinetics. In this direction, the use of electrocatalysts can accelerate the redox kinetics of soluble LiPSs in order to effectively reduce the reaction activation energy and to ensure the capacity contribution. Accordingly, single-atom catalysts,^{23,24} transition metal compounds,^{25–27} and heterostructures,^{28–30} have been widely used in Li–S batteries and exhibited high catalytic activities toward LiPS, thus helping to mitigate the shuttling problem while improving sulfur redox kinetics. However, most of these systems require rather elaborate, multistep synthesis and/or fabrication steps, thus limiting their practical implementation. In this direction, the development of an environmentally friendly electrocatalyst through the recycling of waste materials could offer a sustainable pathway for the development of practical Li–S batteries. Having recognized this challenge, herein, we adopted porous polyisothiocyanurates, named covalent isothiocyanurate frameworks (CITCFs), bearing thiourea moieties as binding sites to capture palladium (Pd(II)) from wastewater. After the reduction of captured Pd(II) to Pd nanoparticles (PdNPs) within the CITCF, a highly efficient electrocatalyst, called PdNP-CITCF, was realized (Figure 1a) for the Li–S

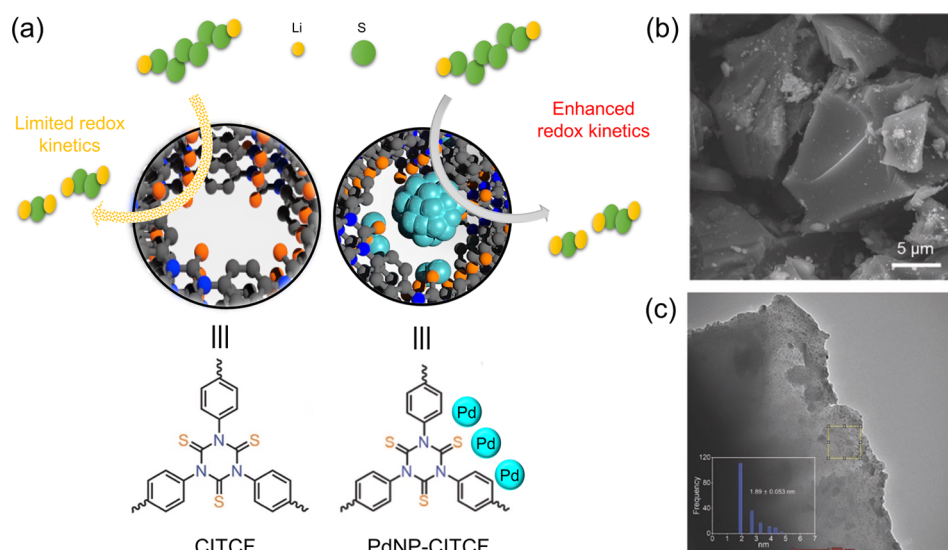


Figure 1. (a) Graphical representation of the effects of CITCF and PdNP-CITCF on the redox kinetics for Li–S batteries along with their chemical structures. (b) SEM image of PdNP-CITCF. (c) TEM image of PdNP-CITCF.

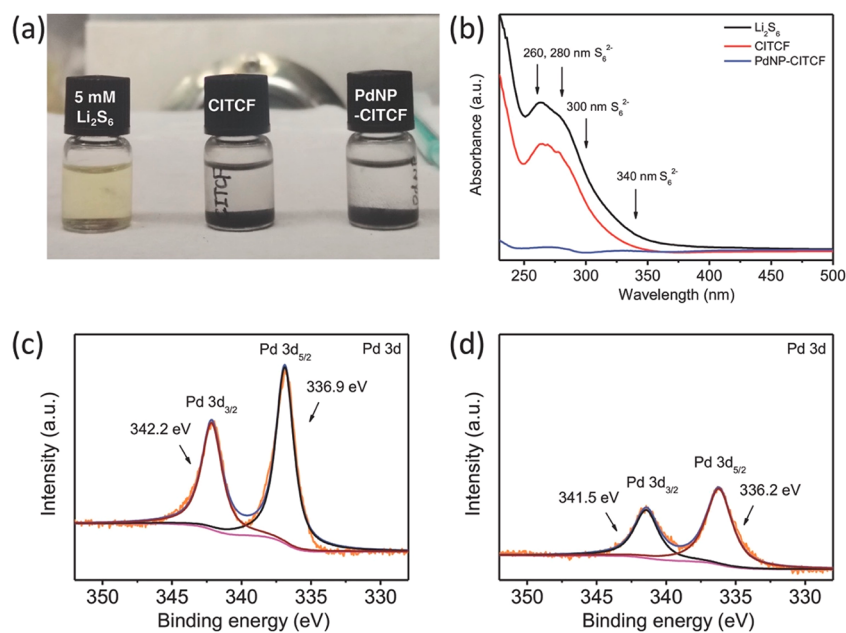


Figure 2. (a) Digital image of the Li-polysulfide (Li₂S₆) adsorption experiment. (b) UV–vis spectra of the Li₂S₆ solution after the adsorption test. (c, d) Pd 3d XPS spectra of PdNP-CITCF before (c) and after (d) adsorption of Li₂S₆.

battery. The PdNP-CITCF provided abundant Pd active sites for anchoring LiPSs via strong chemical bond formation while simultaneously accelerating the conversion of sulfur redox species. Consequently, the as-obtained S@PdNP-CITCF electrode exhibited a high initial specific capacity of 907 mAh g⁻¹ at 1 C, stable capacity of 450 mAh g⁻¹ after 500 cycles at 1 C, and excellent rate performance with a capacity of 681 mAh g⁻¹ at 2 C.

2. RESULTS AND DISCUSSION

We recently reported the synthesis of CITCFs bearing in situ formed isothiocyanate linkages through the trimerization of 1,4-phenylene diisothiocyanate under ionothermal conditions using ZnCl₂ at 500 °C.³¹ The resulting CITCF showed a high BET surface area of 1589 m² g⁻¹ with hierarchical porosity and

a high Pd(II) adsorption capacity of 909 mg g⁻¹ under wastewater conditions.³¹ Subsequent reduction of captured Pd(II) within the polymer network led to the formation of Pd NPs within the CITCF, PdNP-CITCF. Notably, PdNP-CITCF retained a high BET surface area of 1290 m² g⁻¹, thus ensuring the accessibility of the catalytic sites. Scanning electron microscopy (SEM) analysis of CITCF revealed (Figures 1b, S1, and S2) an irregular particle shape and broad particle size distribution. Transmission electron microscopy (TEM) analysis of PdNP-CITCF showed (Figure 1c) homogeneously distributed PdNPs with an average particle diameter of 1.89 nm, which are effectively stabilized within the pores of CITCFs. It is important to note that the average particle size of the PdNPs nicely coincides with the average pore size of CITCFs, thus verifying that homogeneously

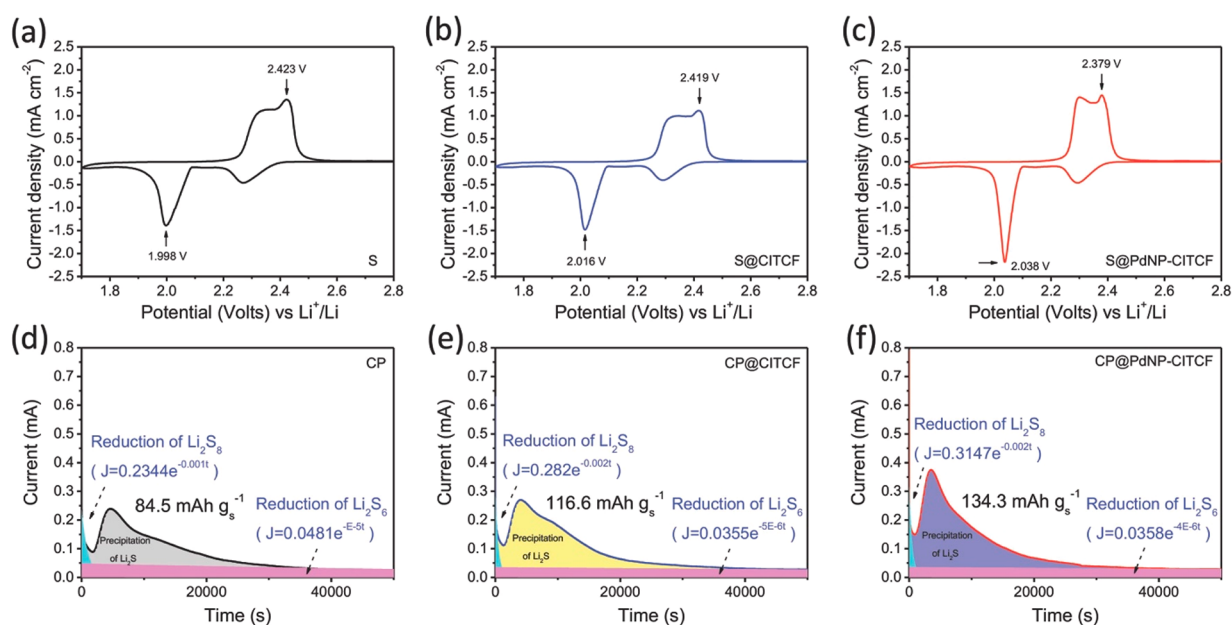


Figure 3. (a–c) CV curves of coin cells with S, S@CITCF, and S@PdNP-CITCF cathodes. (d–f) Potentiostatic discharge profiles of Li₂S nucleation at 2.05 V on different electrodes with the Li₂S₈ catholyte.

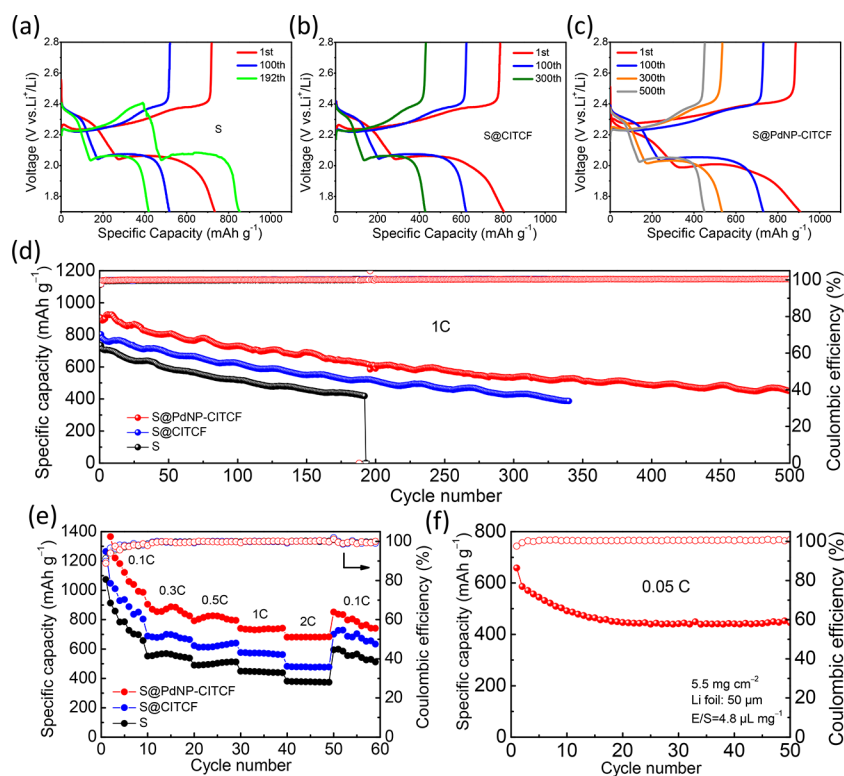


Figure 4. (a–c) Charge–discharge profiles of Li–S batteries with different cathodes at 1 C. (d) Cycling performance at 1 C over 500 cycles of the S, S@CITCF, and S@PdNP-CITCF cathodes with a sulfur loading of 1 mg cm⁻². (e) Rate performance of different cathodes. (f) Cycling performance of the S@PdNP-CITCF cathode with sulfur loading of 5.5 mg cm⁻² at 0.05 C under lean electrolyte conditions (E/S = 4.8 μL mg⁻¹).

distributed sulfur atoms present high affinity binding sites for PdNPs.

The high surface area of PdNP-CITCF prompted us to test static LiPS adsorption, which is rather important to evaluate the affinity of porous materials toward LiPS and to inhibit the shuttling effect. A total of 20 mg of CITCF and PdNP-CITCF were separately added (Figure 2a) into a 0.005 M Li₂S₆ solution. After resting for 3 h, whereas the solution with

CITCF still showed a significant amount of Li₂S₆, the one with PdNP-CITCF became colorless, demonstrating much stronger sulfur immobilization in the case of PdNP-CITCF. Each solution was diluted 10 times after the adsorption test and used for quantitative comparison using ultraviolet–visible (UV–vis) spectroscopy analysis (Figure 2b).

The Li₂S₆ solution exposed to PdNP-CITCF displayed near quantitative uptake as evidenced from the UV–vis absorption

spectrum, whereas the CITCF one showed only 28% reduction in the adsorption intensity, thus clearly confirming the strong affinity of PdNP-CITCF toward Li_2S_6 . The PdNP-CITCF after the absorption test was collected and dried for X-ray photoelectron spectroscopy (XPS) analysis (Figure S3). As shown in Figure 2c,d, the Pd $3d_{3/2}$ and Pd $3d_{5/2}$ peaks at 342.2 and 336.9 eV shifted toward lower binding energies of 341.5 and 336.2 eV, respectively, after Li_2S_6 adsorption, which further confirmed the strong chemical interaction between PdNP and polysulfides.³² In addition, the S 2p spectrum showed the characteristic peaks of PdNP-CITCF before the adsorption of LiPSs.³¹ Following exposure to the Li_2S_6 solution, the formation of sulfate (170.2 eV), polythionate (169.2 eV), and S^{2-} (160.9 eV) originating from the oxidation of polysulfides^{29,33} was observed, which provides the first indication that PdNP-CITCF can not only anchor LiPSs but also modulate their redox kinetics (Figure S4).

Polysulfide redox kinetics were evaluated using cyclic voltammetry (CV) to probe the electrocatalytic activity of PdNP-CITCF. We observed (Figure 3a–c) two pairs of stable redox peaks in S, S@CITCF, and S@PdNP-CITCF electrodes, which were assigned to the reduction of S_8 to soluble long-chain LiPSs (Li_2S_x , $4 \leq x \leq 8$) and to the subsequent formation of insoluble $\text{Li}_2\text{S}_2/\text{Li}_2\text{S}$. In the CV curves, the S@PdNP-CITCF electrode exhibited the most intense peak current and a cathodic shift (2.038 V) toward a higher potential and the anodic peak (2.379 V) toward a lower potential, compared with S@CITCF (2.016 and 2.419 V) and S (1.998 and 2.423 V) electrodes. These results suggest the faster redox kinetics of LiPSs by the introduction of PdNP-CITCF. Furthermore, the kinetics of liquid–liquid redox reactions of LiPSs can be revealed by CV in symmetric cells with Li_2S_6 and Li_2S_6 -free catholytes. CV curves of different electrodes were recorded (Figure S5) in the voltage range -1.0 – 1.0 V. As expected, carbon paper (CP) without Li_2S_6 showed a near-zero capacitive current. The CP@PdNP-CITCF electrode on the other hand exhibited the lowest oxidation potential compared with CP and CP@CITCF electrodes, indicating faster redox kinetics and higher reversibility.

The kinetic analysis of liquid–solid conversion was performed by Li_2S nucleation tests. On the basis of Faraday's law, the calculated capacity of the precipitation of Li_2S on CP@PdNP-CITCF was found to be 134.3 mAh g^{-1} , which was higher than those of CP@CITCF (116.6 mAh g^{-1}) and CP (84.5 mAh g^{-1}), reflecting that PdNP-CITCF can provide more active sites to catalyze the liquid–solid reactions and facilitate efficient Li_2S nucleation (Figure 3d–f).

In order to investigate the electrochemical performance of the electrodes, galvanostatic charge–discharge profiles were recorded. The charge/discharge curves displayed (Figure 4a–c) one charge plateau and two discharge plateaus in agreement with the CV profiles and multistep sulfur redox reaction mechanism. The S@PdNP-CITCF cathode was also characterized by XRD, TEM, and EDS analyses as shown in Figures S6–S8. The cycling performance of Li–S cells with S, S@CITCF, and S@PdNP-CITCF cathodes at 1 C (1675 mA g^{-1}) is shown in Figure 4d based on the sulfur and single-walled carbon nanotubes (SWCNTs) by the ratio of 7:3 (Figure S9). The sulfur loading of each electrode was about 1 mg cm^{-2} . The first discharge capacity of the S@PdNP-CITCF cathode was found to be 907 mAh g^{-1} . In contrast, the S@CITCF and S cathodes delivered lower discharge capacities of 804 and 734 mAh g^{-1} , respectively. After 500 cycles, the capacity for the S@

PdNP-CITCF cathode still retained a discharge capacity of 450 mAh g^{-1} with the retention of 50%, whereas the S@CITCF cathode delivered a much faster capacity decay and a low discharge capacity of 387 mAh g^{-1} after only 340 cycles. In comparison, the control S cathode can only run for 192 cycles, where the charging curve failed to achieve the cutoff voltage of 2.8 V owing to the detrimental shuttling effect and internal short-circuit. Diffusion coefficients of different cathodes were measured by the CV method and electrochemical impedance spectroscopy (EIS) method, as shown in Figures S10 and S11. S 2p XPS spectra of S@PdNP-CITCF cathodes at different states were also compared (Figure S12). EIS analysis of the S@PdNP-CITCF cathode before cycling presented a lower charge transfer resistance (R_{ct}) compared to both S@CITCF and bare S cathodes. In addition, the S@PdNP-CITCF cathode also enabled the steepest Warburg slope after 50 cycles, indicating fast Li^+ diffusion and high catalytic activity (Figure S13). The impact of the PdNP-CITCF amount in the cathodes was also compared as shown in Figure S14.

Rate performance was also evaluated with different cathodes, as shown in Figures 4e and S15. The S@PdNP-CITCF cathode delivered specific capacities of 1367, 871, 804, 735, and 681 mAh g^{-1} at 0.1, 0.3, 0.5, 1, and 2 C, respectively, which are far superior to those with S@CITCF (1048, 682, 612, 575, and 479 mAh g^{-1}) and S (914, 555, 490, 449, and 378 mAh g^{-1}) cathodes. As the current rate comes back to 0.1 C, a specific capacity of 837 mAh g^{-1} was recovered with the S@PdNP-CITCF cathode, while the S@CITCF and S cathodes only delivered 727 and 599 mAh g^{-1} , respectively, suggesting the effectiveness of S@PdNP-CITCF in inhibiting the shuttle effect and enhancing reaction kinetics of LiPS. The voltage gap, ΔE , between the oxidation and the second reduction plateaus refers to a hysteresis in the redox reaction. The S@PdNP-CITCF cathode showed a significantly lower polarization potential ($\Delta E = 163$ and 286 mV) than S@CITCF ($\Delta E = 216$ and 404 mV) and S ($\Delta E = 257$ and 457 mV) cathodes at 0.3 and 2 C (Figure S16). In addition, the S@PdNP-CITCF cathode also exhibited a lower potential barrier in the charging process at 0.3 C, corresponding to the reduced activation energy for the conversion of Li_2S to Li_2S_n (Figure S17). Even with a high sulfur loading of 3.7 mg cm^{-2} and an E/S ratio of $21.6 \mu\text{L mg}^{-1}$, the S@PdNP-CITCF cathode exhibited an initial reversible capacity of 583 mAh g^{-1} and a capacity retention of 59% after 50 cycles at 0.05 C (Figures S18 and S19). High sulfur loading (5.5 mg cm^{-2}) S@PdNP-CITCF cathode under lean electrolyte conditions (E/S ratio of $4.8 \mu\text{L mg}^{-1}$) was also measured as shown in Figure 4f. The comparison of the electrochemical performance of the Pd-based cathode/interlayers is summarized in Table S1.

3. CONCLUSIONS

In summary, we introduced an environmentally friendly approach to develop a sustainable porous electrocatalyst by using recycled Pd from waste materials to enhance the LiPS conversion kinetics in Li–S batteries. The PdNP-CITCF electrocatalyst with high porosity and abundant Pd active sites combines the advantages of strong LiPSs anchoring ability and high electrocatalytic activity, thus effectively boosting Li–S battery performance. This work presents a sustainable approach for the porous electrocatalyst design and deepens our understanding of multielectron sulfur redox processes toward the realization of practical Li–S batteries.

4. EXPERIMENTAL METHODS

4.1. Synthesis and Preparation of CITCF and PdNP-CITCF.

The samples were prepared by following the procedures in the previous literature.³¹ The amount of Pd nanoparticles in the PdNP-CITCF was 8.1 wt %.

4.2. Preparation of S@PdNP-CITCF, S@CITCF, and S Cathodes. Sulfur and single-walled carbon nanotubes (SWCNTs) were mixed at a 7:3 mass ratio and then heated at 160 °C for 12 h. The S cathode was fabricated by mixing the 80 wt % sulfur–SWCNTs hybrid with 10 wt % Ketjen Black (KB) and 10 wt % polyvinylidene fluoride (PVDF) dissolved in *N*-methyl-2-pyrrolidone (NMP), which was then blade-casted on carbon-coated aluminum foil and dried at 60 °C under a vacuum for 10 h. For the S@PdNP-CITCF and S@CITCF cathodes, the sulfur–SWCNTs hybrid and PdNP-CITCF or CITCF were uniformly mixed at a 95:5 mass ratio. The loading of sulfur in each electrode was about 1 mg cm⁻², and the electrolyte amount was 40 μL for each cell.

4.3. Preparation of the High-Loading S@PdNP-CITCF Cathode. The ratio of sulfur–SWCNTs to PdNP-CITCF was set at 95:5 by weight and then evenly mixed with Super P and polytetrafluoroethylene (PTFE) at a 6:2:2 mass ratio. Then, the composite cathode was evenly dispersed on carbon-coated aluminum foil and pressed at 500 MPa. The sulfur loading was 3.7 mg cm⁻², and the electrolyte amount was 80 μL. For the cell with a low E/S ratio of 4.8 μL mg⁻¹, the sulfur loading was 5.5 mg cm⁻² and the electrolyte amount was 30 μL. The cells were cycled at 0.05 C between 1.7 and 2.7 V.

4.4. Li₂S₆ Adsorption Test. The Li₂S₆ solution was prepared by mixing sulfur and lithium disulfide (the molar ratio is 5:1) in a commercial electrolyte (1 M LiTFSI in DOL:DME (1:1 by volume) with 2 wt % LiNO₃) under vigorous stirring. Then, 20 mg of PdNP-CITCF and CITCF were separately added into 0.005 M Li₂S₆ solution, which rested for 3 h. After the adsorption test, the above solutions were diluted to 0.5 mM for UV–vis analysis.

4.5. Li₂S Nucleation Test. The 0.4 M Li₂S₈ electrolyte was prepared by mixing sulfur and lithium disulfide (the molar ratio is 7:1) in tetraglyme under vigorous stirring. Then, 0.5 M LiTFSI was added and stirred for 2 h. The 12 mm carbon fiber papers (CPs) were punched as the substrate to load PdNP-CITCF and CITCF (2 mg cm⁻²). A total of 20 μL of Li₂S₈ electrolyte was dropped onto the cathode side, and 20 μL of commercial electrolyte was dropped onto the lithium anode side. The cells were galvanostatically discharged to 2.06 V at a current of 0.134 mA and then potentiostatically discharged at 2.05 V for 24 h. The nucleation capacity of Li₂S was calculated on the basis of Faraday's Law.

4.6. Electrochemical Characterizations. Electrochemical impedance spectroscopy (EIS) tests were conducted on a VMP3 electrochemical workstation (Bio Logic Science Instruments), where in the voltage amplitude was set to 5 mV in the frequency range of 100 kHz to 10 mHz. Cyclic voltammetry (CV) curves of Li–S cells were recorded at a scan rate of 0.05 mV s⁻¹ at a potential range of 1.7–2.8 V by VMP3. CV of the Li₂S₆ symmetric cells was tested between -1.0 to 1.0 V at 0.5 mV s⁻¹. A 20 μL portion of Li₂S₆ (0.5 M) electrolyte was dropped onto CP for each electrode of the symmetric cell.

4.7. Material Characterizations. The morphological information was characterized by field emission scanning electron microscopy (FE-SEM, Tescan Mira3 LM FE) and transmission electron microscopy (TEM, FEI Tecnai Spirit). Ultraviolet visible (UV–vis) spectroscopy analysis was performed using a Lambda 25 UV–vis spectrophotometer (PerkinElmer, Switzerland). X-ray photoelectron spectroscopy (XPS) measurements were conducted on a VG ESCALAB 220iXL spectrometer (Thermo Fisher Scientific) using focused monochromatized Al K α radiation (1486.6 eV) with a beam size of ~500 μm² (power of 150 W).

■ ASSOCIATED CONTENT

Supporting Information

The Supporting Information is available free of charge at <https://pubs.acs.org/doi/10.1021/acs.chemmater.3c00544>.

Li₂S₆ adsorption test, Li₂S nucleation test, XRD, TEM, and EDS of the cathode, XPS, EIS, CV, and cycling performances, and comparison (PDF)

■ AUTHOR INFORMATION

Corresponding Author

Ali Coskun – Department of Chemistry, University of Fribourg, Fribourg 1700, Switzerland; orcid.org/0000-0002-4760-1546; Email: ali.coskun@unifr.ch

Authors

Tianhong Zhou – Department of Chemistry, University of Fribourg, Fribourg 1700, Switzerland; orcid.org/0000-0002-9537-8465

Yan Zhao – Department of Chemistry, University of Fribourg, Fribourg 1700, Switzerland; orcid.org/0000-0001-5324-5050

Kyung Seob Song – Department of Chemistry, University of Fribourg, Fribourg 1700, Switzerland

Dominika Baster – Electrochemistry Laboratory, Paul Scherrer Institut, Villigen 5232, Switzerland; orcid.org/0000-0002-6732-0565

Mario El Kazzi – Electrochemistry Laboratory, Paul Scherrer Institut, Villigen 5232, Switzerland; orcid.org/0000-0003-2975-0481

Complete contact information is available at:

<https://pubs.acs.org/doi/10.1021/acs.chemmater.3c00544>

Author Contributions

[§](T.Z., Y.Z., and K.S.S.) These authors contributed equally. The manuscript was written through contributions of all authors. All authors have given approval to the final version of the manuscript.

Notes

The authors declare no competing financial interest.

■ ACKNOWLEDGMENTS

A.C. acknowledges the support from the Swiss National Science Foundation (SNF) for funding of this research (200021-188572).

■ REFERENCES

- (1) Choi, J. W.; Aurbach, D. Promise and reality of post-lithium-ion batteries with high energy densities. *Nat. Rev. Mater.* **2016**, *1*, 16013.
- (2) Armand, M.; Tarascon, J.-M. Building better batteries. *Nature* **2008**, *451* (7179), 652–657.
- (3) Goodenough, J. B. Evolution of strategies for modern rechargeable batteries. *Acc. Chem. Res.* **2013**, *46* (5), 1053–1061.
- (4) Wang, Z.; Liu, J.; Wang, M.; Shen, X.; Qian, T.; Yan, C. Toward safer solid-state lithium metal batteries: a review. *Nanoscale Adv.* **2020**, *2* (5), 1828–1836.
- (5) Ji, X.; Nazar, L. F. Advances in Li–S batteries. *J. Mater. Chem.* **2010**, *20* (44), 9821–9826.
- (6) Ji, X.; Lee, K. T.; Nazar, L. F. A highly ordered nanostructured carbon–sulphur cathode for lithium–sulphur batteries. *Nat. Mater.* **2009**, *8* (6), 500–506.
- (7) Manthiram, A.; Fu, Y.; Su, Y.-S. Challenges and prospects of lithium–sulfur batteries. *Acc. Chem. Res.* **2013**, *46* (5), 1125–1134.

- (8) Bhargava, A.; He, J.; Gupta, A.; Manthiram, A. Lithium-sulfur batteries: attaining the critical metrics. *Joule* **2020**, *4* (2), 285–291.
- (9) Liu, J.; Cao, Y.; Zhou, J.; Wang, M.; Chen, H.; Yang, T.; Sun, Y.; Qian, T.; Yan, C. Interfaces Artificial lithium isopropyl-sulfide macromolecules as an ion-selective interface for long-life lithium-sulfur batteries. *ACS Appl. Mater. Interfaces* **2020**, *12* (49), 54537–54544.
- (10) Tian, J. H.; Jiang, T.; Wang, M.; Hu, Z.; Zhu, X.; Zhang, L.; Qian, T.; Yan, C. In situ/operando spectroscopic characterizations guide the compositional and structural design of lithium-sulfur batteries. *Small Methods* **2020**, *4* (6), 1900467.
- (11) Zhou, G.; Li, L.; Wang, D. W.; Shan, X. y.; Pei, S.; Li, F.; Cheng, H. M. A flexible sulfur-graphene-polypropylene separator integrated electrode for advanced Li-S batteries. *Adv. Mater.* **2015**, *27* (4), 641–647.
- (12) Zheng, J.; Tian, J.; Wu, D.; Gu, M.; Xu, W.; Wang, C.; Gao, F.; Engelhard, M. H.; Zhang, J.-G.; Liu, J.; Xiao, J. Lewis acid-base interactions between polysulfides and metal organic framework in lithium sulfur batterie. *Nano Lett.* **2014**, *14* (5), 2345–2352.
- (13) He, Y.; Chang, Z.; Wu, S.; Qiao, Y.; Bai, S.; Jiang, K.; He, P.; Zhou, H. Simultaneously inhibiting lithium dendrites growth and polysulfides shuttle by a flexible MOF-based membrane in Li-S batteries. *Adv. Energy Mater.* **2018**, *8* (34), 1802130.
- (14) Bai, S.; Liu, X.; Zhu, K.; Wu, S.; Zhou, H. Metal-organic framework-based separator for lithium-sulfur batteries. *Nat. Energy* **2016**, *1*, 16094.
- (15) Zhang, B.; Qin, X.; Li, G.; Gao, X. Enhancement of long stability of sulfur cathode by encapsulating sulfur into micropores of carbon spheres. *Energy Environ. Sci.* **2010**, *3* (10), 1531–1537.
- (16) Schuster, J.; He, G.; Mandlmeier, B.; Yim, T.; Lee, K. T.; Bein, T.; Nazar, L. F. Spherical ordered mesoporous carbon nanoparticles with high porosity for lithium-sulfur batteries. *Angew. Chem., Int. Ed.* **2012**, *51* (15), 3591–3595.
- (17) Zheng, G.; Yang, Y.; Cha, J. J.; Hong, S. S.; Cui, Y. Hollow carbon nanofiber-encapsulated sulfur cathodes for high specific capacity rechargeable lithium batteries. *Nano Lett.* **2011**, *11* (10), 4462–4467.
- (18) Guo, J.; Xu, Y.; Wang, C. Sulfur-impregnated disordered carbon nanotubes cathode for lithium-sulfur batteries. *Nano Lett.* **2011**, *11* (10), 4288–4294.
- (19) Wei Seh, Z.; Li, W.; Cha, J. J.; Zheng, G.; Yang, Y.; McDowell, M. T.; Hsu, P.-C.; Cui, Y. Sulphur-TiO₂ yolk-shell nanoarchitecture with internal void space for long-cycle lithium-sulphur batteries. *Nat. Commun.* **2013**, *4*, 1331.
- (20) Han, X.; Xu, Y.; Chen, X.; Chen, Y.-C.; Weadock, N.; Wan, J.; Zhu, H.; Liu, Y.; Li, H.; Rubloff, G.; et al. Reactivation of dissolved polysulfides in Li-S batteries based on atomic layer deposition of Al₂O₃ in nanoporous carbon cloth. *Nano Energy* **2013**, *2* (6), 1197–1206.
- (21) Li, Z.; Zhang, J.; Lou, X. W. Hollow carbon nanofibers filled with MnO₂ nanosheets as efficient sulfur hosts for lithium-sulfur batteries. *Angew. Chem., Int. Ed.* **2015**, *54* (44), 12886–12890.
- (22) Tao, Y.; Wei, Y.; Liu, Y.; Wang, J.; Qiao, W.; Ling, L.; Long, D. Kinetically-enhanced polysulfide redox reactions by Nb₂O₅ nanocrystals for high-rate lithium-sulfur battery. *Energy Environ. Sci.* **2016**, *9* (10), 3230–3239.
- (23) Du, Z.; Chen, X.; Hu, W.; Chuang, C.; Xie, S.; Hu, A.; Yan, W.; Kong, X.; Wu, X.; Ji, H.; Wan, L.-J. Cobalt in nitrogen-doped graphene as single-atom catalyst for high-sulfur content lithium-sulfur batteries. *J. Am. Chem. Soc.* **2019**, *141* (9), 3977–3985.
- (24) Liu, G.; Wang, W.; Zeng, P.; Yuan, C.; Wang, L.; Li, H.; Zhang, H.; Sun, X.; Dai, K.; Mao, J.; et al. Strengthened d-p Orbital Hybridization through Asymmetric Coordination Engineering of Single-Atom Catalysts for Durable Lithium-Sulfur Batteries. *Nano Lett.* **2022**, *22* (15), 6366–6374.
- (25) Li, Z.; He, Q.; Xu, X.; Zhao, Y.; Liu, X.; Zhou, C.; Ai, D.; Xia, L.; Mai, L. A 3D NitrogenDoped Graphene/TiN Nanowires Composite as a Strong Polysulfide Anchor for Lithium-Sulfur Batteries with Enhanced Rate Performance and High Areal Capacity. *Adv. Mater.* **2018**, *30* (45), 1804089.
- (26) Zhou, T.; Zhao, Y.; Zhou, G.; Lv, W.; Sun, P.; Kang, F.; Li, B.; Yang, Q.-H. An in-plane heterostructure of graphene and titanium carbide for efficient polysulfide confinement. *Nano Energy* **2017**, *39*, 291–296.
- (27) Shen, Z.; Jin, X.; Tian, J.; Li, M.; Yuan, Y.; Zhang, S.; Fang, S.; Fan, X.; Xu, W.; Lu, H.; et al. Cation-doped ZnS catalysts for polysulfide conversion in lithium-sulfur batteries. *Nat. Catal.* **2022**, *5* (6), 555–563.
- (28) Zhou, T.; Lv, W.; Li, J.; Zhou, G.; Zhao, Y.; Fan, S.; Liu, B.; Li, B.; Kang, F.; Yang, Q.-H. Twinborn TiO₂-TiN heterostructures enabling smooth trapping-diffusion-conversion of polysulfides towards ultralong life lithium-sulfur batteries. *Energy Environ. Sci.* **2017**, *10* (7), 1694–1703.
- (29) Zhang, L.; Liu, Y.; Zhao, Z.; Jiang, P.; Zhang, T.; Li, M.; Pan, S.; Tang, T.; Wu, T.; Liu, P.; et al. Enhanced polysulfide regulation via porous catalytic V₂O₃/V₃C₇ heterostructures derived from metal-organic frameworks toward high-performance Li-S batteries. *ACS Nano* **2020**, *14* (7), 8495–8507.
- (30) Wang, R.; Luo, C.; Wang, T.; Zhou, G.; Deng, Y.; He, Y.; Zhang, Q.; Kang, F.; Lv, W.; Yang, Q. H. Bidirectional catalysts for liquid-solid redox conversion in lithium-sulfur batteries. *Adv. Mater.* **2020**, *32* (32), 2000315.
- (31) Song, K. S.; Ashirov, T.; Talapaneni, S. N.; Clark, A. H.; Yakimov, A. V.; Nachtegaal, M.; Copéret, C.; Coskun, A. Porous polyisothiocyanurates for selective palladium recovery and heterogeneous catalysis. *Chem.* **2022**, *8* (7), 2043–2059.
- (32) Li, W.; Qian, J.; Zhao, T.; Ye, Y.; Xing, Y.; Huang, Y.; Wei, L.; Zhang, N.; Chen, N.; Li, L.; et al. Boosting High-Rate Li-S Batteries by an MOF-Derived Catalytic Electrode with a Layer-by-Layer Structure. *Adv. Sci.* **2019**, *6* (16), 1802362.
- (33) Liang, X.; Kwok, C. Y.; Lodi-Marzano, F.; Pang, Q.; Cuisinier, M.; Huang, H.; Hart, C. J.; Houtarde, D.; Kaup, K.; Sommer, H.; et al. Tuning transition metal oxide-sulfur interactions for long life lithium sulfur batteries: the “Goldilocks” principle. *Adv. Energy Mater.* **2016**, *6* (6), 1501636.